Geophysical Research Letters

RESEARCH LETTER
10.1029/2025GL116716

Hadley Cell Instability and Its Link to Tropical Depression-Type Waves

Qiao-Jun Lin[1], **Ángel F. Adames Corraliza**[1], **and Víctor C. Mayta**[1]

[1]Department of Atmospheric and Oceanic Sciences, University of Wisconsin, Madison, WI, USA

Key Points:

- A diagnostic metric is developed based on recent theory on the interaction between tropical depression (TD)-type waves and the Hadley Cell
- The instability metric captures the location and timing of strong TD-type wave activity in ERA5 data
- Coupled Model Intercomparison Project Phase 6 models with higher instability metric exhibit stronger TD moisture variance and poleward eddy moisture flux in the Northern Hemisphere

Supporting Information:

Supporting Information may be found in the online version of this article.

Correspondence to:

Q.-J. Lin,
qiaojun.lin@wisc.edu

Citation:

Lin, Q.-J., Adames Corraliza, Á. F., & Mayta, V. C. (2025). Hadley Cell instability and its link to tropical depression-type waves. *Geophysical Research Letters*, *52*, e2025GL116716. https://doi.org/10.1029/2025GL116716

Received 25 APR 2025
Accepted 15 SEP 2025

Author Contributions:

Conceptualization: Qiao-Jun Lin, Ángel F. Adames Corraliza, Víctor C. Mayta
Formal analysis: Qiao-Jun Lin, Ángel F. Adames Corraliza, Víctor C. Mayta
Supervision: Qiao-Jun Lin, Ángel F. Adames Corraliza, Víctor C. Mayta
Writing – review & editing: Qiao-Jun Lin, Ángel F. Adames Corraliza, Víctor C. Mayta

Abstract A recent theory proposes that tropical depression (TD)-type waves grow by flattening the mean meridional moisture gradient, consequently weakening the Hadley Cell through a poleward moisture flux. To evaluate this theory, we investigate the seasonality of TD-type waves and their relation to the Hadley Cell in ERA5 and Coupled Model Intercomparison Project Phase 6 (CMIP6) models. On the basis of the theory, a Hadley Cell instability metric is defined whose variability is largely determined by the background meridional moisture gradient and the sensitivity of rainfall to moisture fluctuations. Results show that both TD-type wave column moisture variance and eddy moisture fluxes peak when the Hadley Cell instability metric is a maximum. These conditions typically occur when the mean meridional precipitation gradient is strongest and the Hadley Cell is weak and narrow. CMIP6 models that exhibit higher Hadley Cell instability metric simulate stronger TD-type wave activity in the Northern Hemisphere.

Plain Language Summary Tropical depression (TD)-type waves are synoptic-scale disturbances that play an important role in the hydrological cycle of many off-equatorial regions and are often seeds for tropical cyclones. Despite decades of research, our understanding of the existence and core processes of TD-type waves remains limited. A recently developed theory posits these waves as instabilities that grow by stirring the horizontal distribution of moisture and weakening the Hadley Cell. Here, we demonstrate that in reanalysis and climate models, the amplitude, seasonality, and moisture transports associated with TD-type waves align with the Hadley Cell instability metric, as described in previous studies.

1. Introduction

Convectively coupled tropical depression (TD)-type waves are synoptic-scale disturbances that are closely connected with cumulus convection (Cheng et al., 2023; Kiladis et al., 2009; Lau & Lau, 1990; Takayabu, 1994). In the Northern Hemisphere, TD-type waves propagate westward or northwestward over oceans (Lau & Lau, 1990; Lubis & Jacobi, 2015; Rydbeck & Maloney, 2015; Takayabu & Nitta, 1993; Vargas Martes et al., 2023). They play an important role in the hydrologic cycle of the regions they traverse, can sometimes cause floods, and serve as seeds for tropical cyclone development over the Pacific and Atlantic Oceans (e.g., Avila et al., 2000; Dominguez et al., 2020; Frank & Roundy, 2006; Huang & Huang, 2011; Landsea, 1993; Lubis & Jacobi, 2015; Russell et al., 2017; Serra et al., 2010; A. H. Sobel & Bretherton, 1999; Yoshida & Ishikawa, 2013).

TD-type waves are distinct as they do not correspond to any mode of Matsuno's linear equatorial wave theory (Matsuno, 1966; Wheeler & Kiladis, 1999). Even though they have been studied for decades (e.g., Riehl, 1945), there is no agreed-upon theory that describes their existence, structure, and growth. Furthermore, it is well known that TD-type waves are primarily a Northern Hemisphere summer feature. While this is attributed to the fact that the Intertropical Convergence Zone (ITCZ) is north of the equator (Frank & Roundy, 2006; Huang & Huang, 2011), there remains no consensus on the physical processes that explain their preponderance over the Northern Hemisphere's oceans.

Despite differences in geographical basic states and structures (Kiladis et al., 2009; Lau & Lau, 1990; Mayta & Adames Corraliza, 2024; Mayta et al., 2025; Reed & Recker, 1971; Rydbeck & Maloney, 2014; Shapiro, 1986; Vargas Martes et al., 2023), oceanic TD-type waves are primarily driven by the same thermodynamic processes. Diabatic heating and adiabatic cooling approximately balance each other, resulting in weak temperature gradient (WTG) balance (A. H. Sobel et al., 2001). Further, temperature variations in the waves are smaller than moisture fluctuations (Luo et al., 2023; Mayta & Adames, 2023; Mayta & Adames Corraliza, 2024; Vargas Martes et al., 2023). Systems that obey these criteria are referred to as “moisture modes” (Raymond & Fuchs, 2009; A. Sobel & Maloney, 2012; Yu & Neelin, 1994). The growth of moisture anomalies in all oceanic TD-type systems is

largely determined by radiative heating and the advection of background moisture by anomalous meridional winds (Mayta & Adames Corraliza, 2024; Rydbeck & Maloney, 2015). The former is associated with upper-tropospheric clouds, which reduce longwave radiative cooling and offset the drying from vertical advection via the WTG approximation (Chikira, 2014; Wolding & Maloney, 2015; Wolding et al., 2016). The latter process was first documented by A. H. Sobel et al. (2001) and was later referred to as moisture-vortex instability (MVI) (Adames, 2021; Adames & Ming, 2018). Recent work has proposed that MVI arises from instabilities in the meridional moisture gradients of the ITCZ, which can be modulated by the lower branch of the Hadley Cell (Adames Corraliza & Mayta, 2024). When TD-type waves grow from MVI, they induce a poleward eddy moisture flux that flattens the moisture gradient, thereby weakening the Hadley Cell.

Despite advances in our understanding of TD-type waves, accurately representing their variability remains a significant challenge for global climate models (GCMs, Camargo, 2013; Daloz et al., 2012; Huang et al., 2013; Ruti & Dell' Aquila, 2010; Vargas Martes et al., 2025). Several studies suggested that this poor representation often originates from inadequate coupling between TD waves and convection (Martin & Thorncroft, 2015; Skinner & Diffenbaugh, 2013). Other studies highlighted the importance of model resolution in realistically simulating TD-type waves (Camargo, 2013; Martin & Thorncroft, 2015; Skinner & Diffenbaugh, 2014). Recently, Vargas Martes et al. (2025) found that climate models that simulate stronger east Pacific easterly waves tend to exhibit weak meridional background moisture gradients, consistent with the idea that these waves act to "stir" column moisture throughout the tropics (Adames Corraliza & Mayta, 2024).

Based on previous findings that suggest TD-type waves originate from instabilities in the lower branch of the Hadley Cell, this study investigates the relationship between these two phenomena using reanalysis data and output from the Coupled Model Intercomparison Project Phase 6 (CMIP6). These analyses aim to address the following key questions:

Q1: How is the TD-type wave variability linked to the Hadley Cell?
Q2: To what extent can global climate models reproduce this association?

The data sets and methods are described in Section 2. Section 3 summarizes the theory that links TD-type variability to Hadley Cell strength. Section 4 diagnoses the relationship between TD-type variability and Hadley Cell instability metric in reanalysis. In Section 5, we apply the same analysis to climate models. Major findings and discussions are summarized in Section 6.

2. Data Description, Processing, and Diagnostics

2.1. Reanalysis and Model Data

The fifth generation of the European Centre for Medium-Range Weather Forecasts reanalysis (ERA5, Hersbach et al., 2019) is used for the 34-year period 1984–2017 to enable analysis of climatological characteristics and comparability with previous studies. It provides daily temporal resolution, a spatial resolution of 0.5° longitude × 0.5° latitude, and 27 pressure levels ranging from 1000 to 100 hPa. ERA5 serves as a reference for evaluating 39 CMIP6 models (Eyring et al., 2016, Table S1 in Supporting Information S1) under the historical scenario from 1984 to 2014. For consistent comparison, all data sets are interpolated to a uniform horizontal resolution of 2.5° longitude × 2.5° latitude following a first-order conservative remapping (Jones, 1999). Variables used include moisture, temperature, geopotential height, horizontal winds, vertical velocity, and precipitation.

2.2. Filtering for Wave Signal

To isolate the TD-type wave signal, the field variables are filtered using fast Fourier transforms (FFT) in space and time to retain wavenumbers $k = -20$ to -5 and periods of 2.5–10 days (denoted by primes $'$). Before performing the FFT, we apply a split-cosine-bell window to reduce the leakage from strong spectral peaks. This window will diminish the wave amplitude at the beginning and end of the data period (Donnelle & Rust, 2005). Thus, the first and last years of the data are excluded.

2.3. Space-Time Spectrum

Space-time spectrum analysis is computed following Wheeler and Kiladis (1999), except that for June–November and December–May (182 and 183 days), we apply 48-day segments overlapping by 15 days (i.e., days 1–48, 34–

81, 67–114, 100–147, and 133–180). This approach yields five segments per season, compared to the two typically obtained using 96-day windows with 30-day overlaps, allowing for a more accurate representation of synoptic-scale variability (Dias & Kiladis, 2014; Dias et al., 2023). Sensitivity tests show that the results are not significantly affected by the choice of segment configuration. The spectra of the half-year period are produced one at a time and then averaged over 32 time frames during the December 1984–November 2016 period. Given our focus on TD-type waves, the spectrum analysis retains only the westward symmetric component.

2.4. Metrics of Hadley Cell Strength

Following Oort and Yienger (1996), we compute the mass-weighted zonal-mean stream function (Ψ) for each month in the data set,

$$\Psi(\phi,p)=\frac{2\pi a\cos\phi}{g}\int_{p}^{p_s}v(\phi,p')\,dp' \tag{1}$$

where a is the global radius of the Earth, g is the gravitational acceleration, ϕ is latitude, and $v(\phi,p')$ is monthly zonal-mean meridional winds. A stronger stream function represents a stronger Hadley circulation. The Hadley Cell strength in the Northern (Southern) Hemisphere is defined as the maximum (minimum) value of Ψ (i.e., Ψ_N and Ψ_S) at 500 hPa between 40°S–40°N (Caballero, 2007; Chemke & Polvani, 2019; Kang et al., 2013; Mitas & Clement, 2005).

3. Theory

According to moisture mode and MVI theories (Adames Corraliza & Mayta, 2024; Ahmed et al., 2021; Mayta & Adames, 2023; Mayta & Adames Corraliza, 2024; Mayta et al., 2022; A. H. Sobel et al., 2001), TD-type waves should exhibit the following characteristics:

3.1. Propagation and Amplitude

For an idealized Hadley Cell on an f-plane in which precipitation (P) is a linear function of column water vapor ($\langle q\rangle$), Adames Corraliza and Mayta (2024) found moisture modes that grow from MVI have a frequency (ϖ_r) and growth rate (ϖ_i) given by:

$$\varpi_r=\overline{u}k\pm\sqrt{\frac{\beta_q k}{2\tau_c K^2}} \tag{2}$$

$$\varpi_i=\pm\sqrt{\frac{\beta_q k}{2\tau_c K^2}} \tag{3}$$

where $\overline{u}$ is the background lower tropospheric wind, $K=\sqrt{k^2+l^2}$ is the horizontal wavenumber, k and l are the zonal and meridional wavenumbers, respectively, τ_c is the convective moisture adjustment timescale, which describes the local sensitivity of precipitation (P) to water vapor (q) fluctuations ($P=\langle q\rangle/\tau_c$), and

$$\beta_q=-\frac{f}{S}\frac{\partial L_v\langle\overline{q}\rangle}{\partial y}(1+r) \tag{4}$$

is a measure of the strength of the mean meridional moisture gradient, where $f=2\Omega\sin\phi$ is the planetary vorticity, S is the gross dry stability (Yu & Neelin, 1994), $\langle\overline{q}\rangle$ is the mean column moisture, and r is the cloud-radiative feedback parameter (Peters & Bretherton, 2005).

Given that the mean state is in WTG balance, vertical motion in the model is also predominantly dependent on $\langle q\rangle$. As the mean vertical motion is associated with the Hadley Cell's mass streamfunction (Ψ), the growth rate of the unstable moisture modes is related to the Hadley Cell and mean rainfall as follows (for a detailed derivation, refer to Section S1 in Supporting Information S1):

$$\varpi_i = \sqrt{\frac{|F_q|k}{2K^2}} \tag{5}$$

where

$$F_q \equiv \frac{\beta_q}{\tau_c} = -\frac{f}{S}\frac{\partial L_v \overline{P}}{\partial y}(1+r) = -\frac{fg}{\Delta p}\frac{\partial^2 \Psi}{\partial y^2} \tag{6}$$

Since S varies little in space and time over the tropics (not shown), and f does not vary in time, F_q is largely determined by the background meridional moisture gradient and τ_c, which are in turn related to variability in Ψ and P.

3.2. Hadley Cell Instability Metric

As shown in Equation 5, since the wavenumbers do not vary in time, temporal variations of the growth rate from MVI comes from F_q. Therefore, we posit that a diagnostic metric based on F_q can be used to diagnose TD-type wave activity, referred to as the Hadley Cell instability metric. While F_q is by construction a constant in the linear theory, the diagnostic form of F_q will be calculated at every grid point. Hence, the diagnostic F_q will vary in space and time. F_q can be either positive or negative, corresponding to instabilities on the poleward and equatorward flanks of the mean rainfall, respectively.

3.3. Relation Between Moisture Variance and Eddy Moisture Flux

Under steady state, the zonally averaged eddy moisture flux $\left(\langle\overline{v'q'}\rangle\right)$ is assumed to be proportional to the zonally averaged eddy moisture variance $\left(\overline{\langle q'\rangle^2}\right)$ through the following relation:

$$\overline{\langle q'\rangle^2} = \tau_F \langle\overline{v'q'}\rangle \tag{7}$$

where

$$\tau_F = -\frac{\tau_c}{\Gamma_e}\frac{\partial\langle\overline{q}\rangle}{\partial y} \tag{8}$$

is a proportionality timescale, and Γ_e is the effective gross moist stability–a measure of the moist static stability of the column–and primes denote TD-type wave-filtered variables. During the hemispheric summer, a shorter τ_c and decreased Γ_e are expected, in association with stronger background convection. Additionally, the poleward downgradient of background moisture weakens compared to winter (see Figure S1 in Supporting Information S1). Therefore, we assume τ_F to vary less than its individual contributions. As a result, a near-linear relation between $\overline{\langle q'\rangle^2}$ and $\langle\overline{v'q'}\rangle$ is expected. Details on the derivation of Equation 7 are shown in Section S2 in Supporting Information S1.

It is worth noting that a correlation between $\overline{\langle q'\rangle^2}$ and $\langle\overline{v'q'}\rangle$ does not sufficiently indicate that TD-type waves are instabilities associated with the lower branch of the Hadley Cell. Rather, we expect these quantities to be correlated with each other and also be coherent with F_q. Examining the relationship between $\overline{\langle q'\rangle^2}$, $\langle\overline{v'q'}\rangle$, and F_q is the goal of the next section.

4. Assessment From Reanalysis Data

4.1. Space-Time Spectrum of Column-Integrated Moisture

The suitability of the theory outlined here is first examined by comparing the dispersion relation in Equation 2 to the global signal of TD-type waves. Figure 1 shows a space-time signal obtained by dividing the column moisture's power spectrum by its red noise background (Wheeler & Kiladis, 1999). As expected, the strongest signal occurs over the Northern Hemisphere during boreal summer, aligning with the dispersion lines

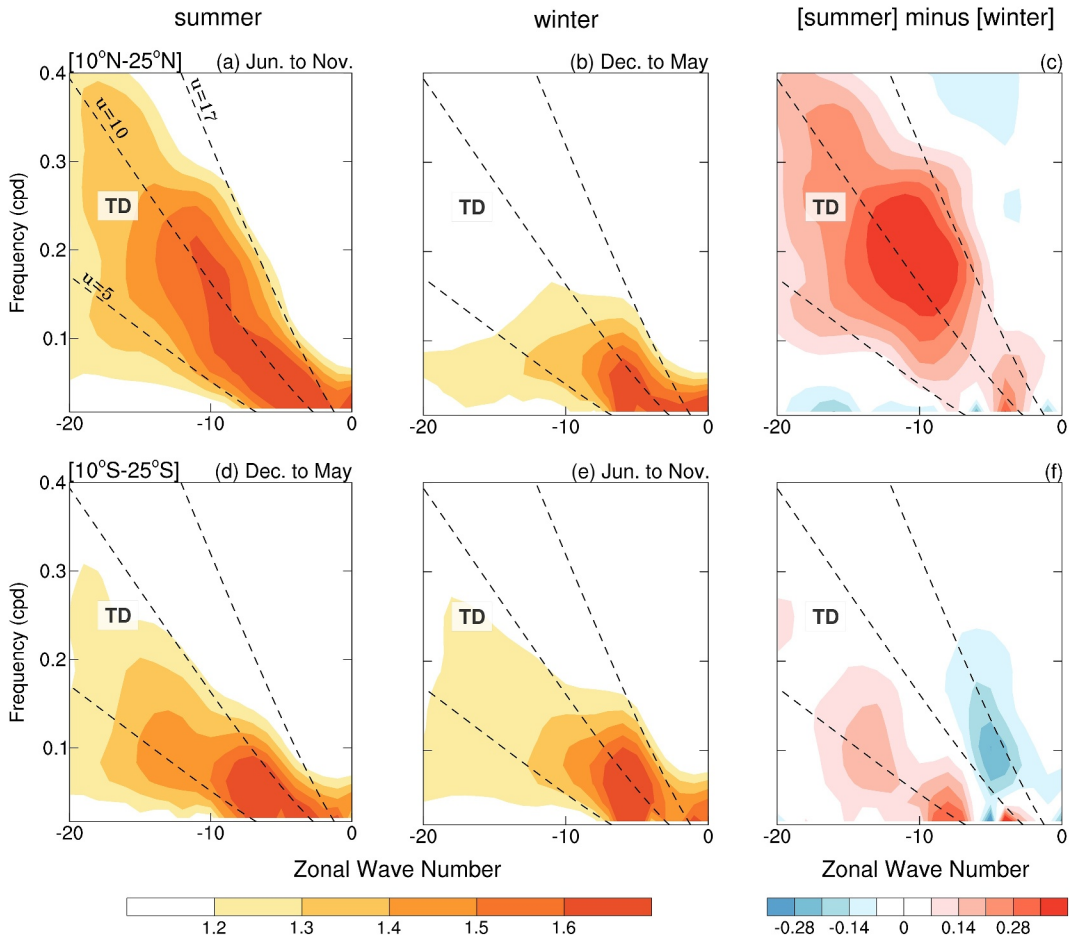

Figure 1. Space-time signal-to-noise ratio of the symmetric component of column-integrated moisture over 10°N–25°N, for (a) the June to November, (b) the December to May, and (c) the difference between summer and winter (a–b). (d–f) As (a–c), but over 10°S–25°S for (d) the December to May, (e) the June to November, and (f) the difference between summer and winter (d–e). The *x*-axis shows westward-propagating zonal wavenumbers. The *y*-axis shows the frequency in cycles per day (cpd). Dashed lines correspond to the tropical depression-type wave dispersion curves obtained from Equation 2 using $\overline{u} = 5$, 10, and 17 m s^{-1} and constants shown in Table S2 in Supporting Information S1, with line labels indicated in panel (a). Color intervals are 0.1 in panels (a, b, d, and e) and 0.07 in panels (c, f), respectively.

corresponding to trade winds ranging from $\overline{u}$ = 5–17 m s^{-1}. Wave activity in this hemisphere exhibits a pronounced seasonality, as the signal nearly vanishes during boreal winter (Figures 1a–1c). In the Southern Hemisphere, the signal is strongest during austral summer for trade winds within 5 and 10 m s^{-1} (Figure 1d). During austral winter, the signal weakens and shifts toward faster speeds (Figures 1e and 1f), consistent with the stronger trade winds seen during this season.

4.2. Coherence Between TD-Type Wave Activity and Instability Metric

Figure 2 shows a map of TD-type wave moisture variance $\left(\sigma_q^2 = \langle L_v q' \rangle^2\right)$, TD-filtered eddy moisture fluxes, and the Hadley Cell instability metric (F_q). We see that TD variance is spatially collocated with a poleward eddy moisture flux, in agreement with the theory. During boreal summer (Figure 2a), the local maxima occur over 10°N–30°N of the eastern Pacific, western Pacific, and Atlantic Ocean, the regions where TD-type wave activity is strongest (e.g., Kiladis et al., 2006; Lau & Lau, 1990; Nitta et al., 1985; A. H. Sobel & Bretherton, 1999). Some activity is also seen in the southern Indian Ocean and southwestern Pacific (5°S–20°S). During austral summer (Figure 2b), the eddy moisture fluxes strengthen over the southern warm pool between 10°S and 30°S, whereas in the Northern Hemisphere these fluxes weaken and shift closer to the equator. Variance near the equator may be increased by other tropical waves (e.g., mixed Rossby–gravity waves; Kiladis et al., 2009). Figure 2 further

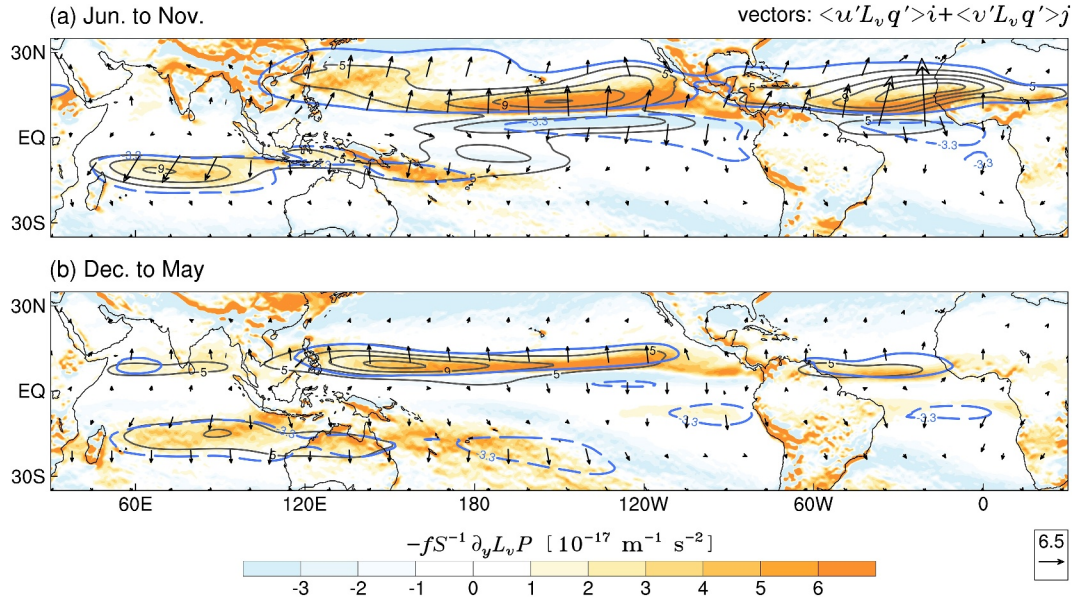

Figure 2. Spatial distribution of the tropical depression (TD)-filtered eddy moisture flux (vectors; $\langle u' L_v q' \rangle \hat{i} + \langle v' L_v q' \rangle \hat{j}$), the Hadley Cell instability metric (shadings; $F_q \equiv -fS^{-1}\partial_y L_v \overline{P}$, Equation 6), variance of TD-type wave-filtered column moisture (black contours; σ_q^2), and TD-filtered meridional eddy moisture flux (blue contours; $\langle v' L_v q' \rangle$), (a) during June–November and (b) during December–May. Primes ($'$) denote TD-filtered variables. Contour interval is 2×10^{13} J^2 m^{-4} for σ_q^2. Contours of $\langle v' L_v q' \rangle$ represent values of $\pm 3.3 \times 10^6$ W m^{-1}. Solid (dashed) blue contours in the Northern (Southern) Hemisphere indicate poleward flux. Shading interval is 1×10^{-17} m^{-1} s^{-2}. The reference vector has a magnitude of 10^6 W m^{-1}.

reveals a coherence between TD-filtered moisture variance and F_q, as well as between poleward eddy moisture flux and F_q. The highest variability occurs on the poleward flank of the ITCZ, in regions of large F_q. This coherence is particularly pronounced in the Northern Hemisphere.

The relationships described above are summarized in Figure 3. We consider the 10°–30° latitude band to isolate regions with the strongest TD-type waves and large positive F_q during summer (refer to Figure 2). In both hemispheres, the relation between TD moisture variance $\left(\sigma_q^2\right)$ and poleward eddy moisture flux ($\langle v' L_v q' \rangle$) is nearly linear, exhibiting a correlation of 0.96 in the Northern Hemisphere and 0.88 in the Southern Hemisphere (Figures 3a and 3b), consistent with the assumptions of Equations 7 and 8. A significant linear correlation is also observed between σ_q^2 and F_q in the Northern Hemisphere ($\gamma = 0.92$, Figure 3c). In the Southern Hemisphere, both F_q and σ_q^2 are smaller and the correlation is slightly weaker ($\gamma = 0.82$, Figure 3d). The weakest σ_q^2 is observed during the hemispheric winter, when negative F_q appears over the 10°–30° oceanic latitude band (see also Figure 2). These negative values reflect a weakening of the F_q values over the poleward edge of the ITCZ as well as the equatorward displacement of extratropical rainfall. The σ_q^2 also shows coherence with other measures of F_q, which relate to Ψ and vertical velocity (refer to Section S1 and Figure S2 in Supporting Information S1). Comparable relationships emerge when analyzing TD-filtered curvature vorticity (see Section S3, Figures S3 and S4 in Supporting Information S1). These findings suggest that the stronger TD-type waves in the Northern Hemisphere are associated with the larger instabilities evident in that hemisphere, as indicated by F_q. In Section S4 in Supporting Information S1 we show that these results are robust to the removal of the seasonal cycle, indicating that $\langle v' L_v q' \rangle$, σ_q^2, and F_q covary at interannual timescales (Figure S5 in Supporting Information S1).

4.3. Linking TD-Type Variability With the Hadley Cell

Up to this point, we have demonstrated that TD-type waves are consistent with viewing them as instabilities of the Hadley Cell. However, we have yet to relate their variability to the strength of the Hadley Cell itself. In Figures 3e and 3f, σ_q^2 is compared with the Hadley Cell's strength (Ψ_N and Ψ_S, Section 2.4), revealing correlations of −0.70 in

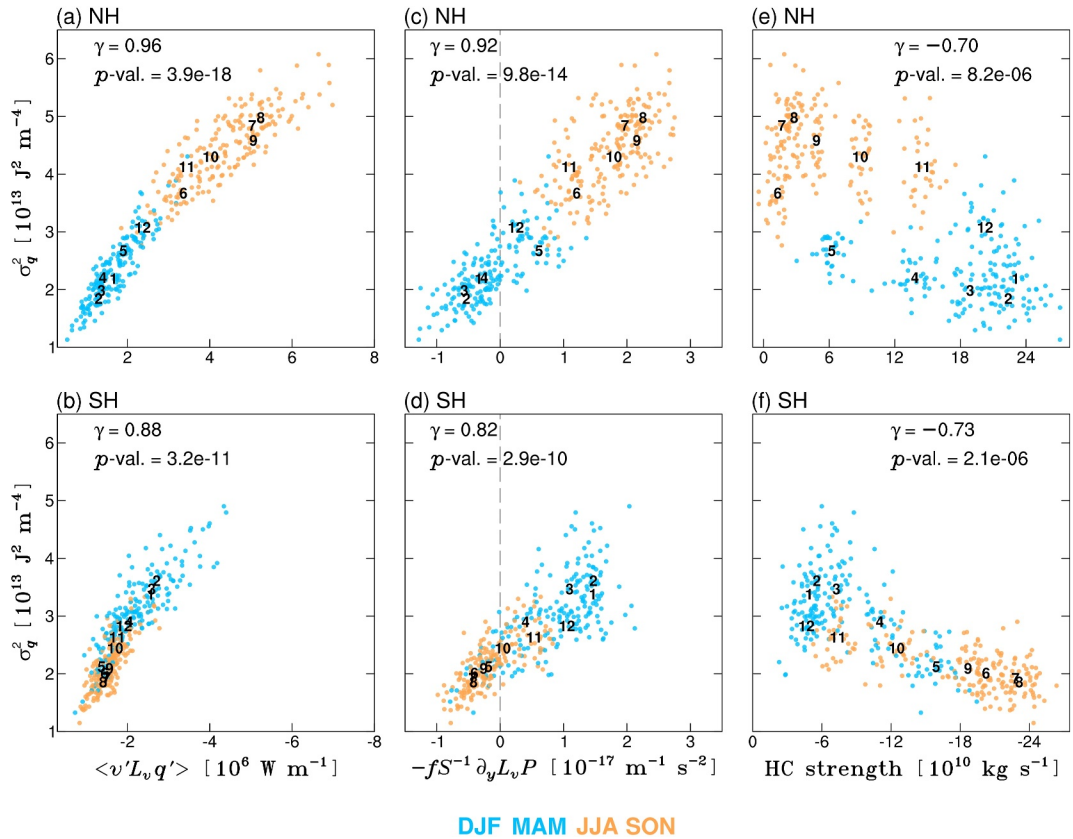

Figure 3. Scatterplots of monthly averages of tropical depression (TD)-filtered meridional eddy moisture flux ($\langle v'L_v q' \rangle$) versus TD-filtered column moisture variances (σ_q^2), averaged over all longitudes and over (a) 10°N–30°N and (b) 10°S–30°S. Primes ($'$) denote TD-filtered variables. As (a, b), but (c, d) for the Hadley Cell instability metric ($-fS^{-1}\partial_y L_v \overline{P}$) versus σ_q^2 and (e, f) for Hadley Cell strength (Equation 1) versus σ_q^2. The colored dots represent individual periods as follows: December–May (DJFMAM, blue) and June–November (JJASON, orange). Numbers denote the monthly climatology from month 1 to 12. Values in the top corner are correlation coefficients (γ) and p-values. Dash lines are 0 m^{-1} s^{-2}.

the Northern Hemisphere and −0.73 in the Southern Hemisphere. This anticorrelation arises because the Hadley Cell narrows as it weakens during summer (Pikovnik et al., 2022; Schneider et al., 2010), which in turn is associated with a large $\partial_y^2 \Psi$ (i.e., a large F_q in Equation 6; refer to Figure S6 in Supporting Information S1). We further find that in the Northern Hemisphere, the highest values of σ_q^2 lag the lowest values of Ψ_N by a month. The one month lagged correlation is −0.91. This one month lag indicates that Ψ reaches a minimum value before the Hadley Cell is at its narrowest. Nonetheless, F_q attains a maximum value when the Hadley Cell is at its narrowest, implying a stronger meridional precipitation gradient and larger TD-type wave variability.

5. Insights From Climate Models

In this section, we assess whether the climate models can simulate the interaction between the TD variability and instability metric. We perform the same analysis as presented in Figures 3a–3d for 39 CMIP6 models and summarize their correlation coefficients in Figure 4. In the Northern Hemisphere (Figure 4a), all models exhibit a high correlation coefficient between σ_q^2 and $\langle v'L_v q' \rangle$ associated with TD-type waves, ranging from 0.87 to 0.97, with a multi-model mean of 0.94 ± 0.02. The simulated TD-type waves also exhibit a strong response to F_q, with an average correlation of 0.86 ± 0.06. Relatively low correlations observed in IPSL-CM6A-LR and IPSL-CM6A-LR-INCA are likely due to their unrealistically weak simulations of easterly waves (Vargas Martes et al., 2025). In the Southern Hemisphere (Figure 4b), σ_q^2 also shows a strong correlation with $\langle v'L_v q' \rangle$, with a multi-model mean of 0.90 ± 0.02. The correlation between σ_q^2 and F_q is consistently above 0.8 across all models

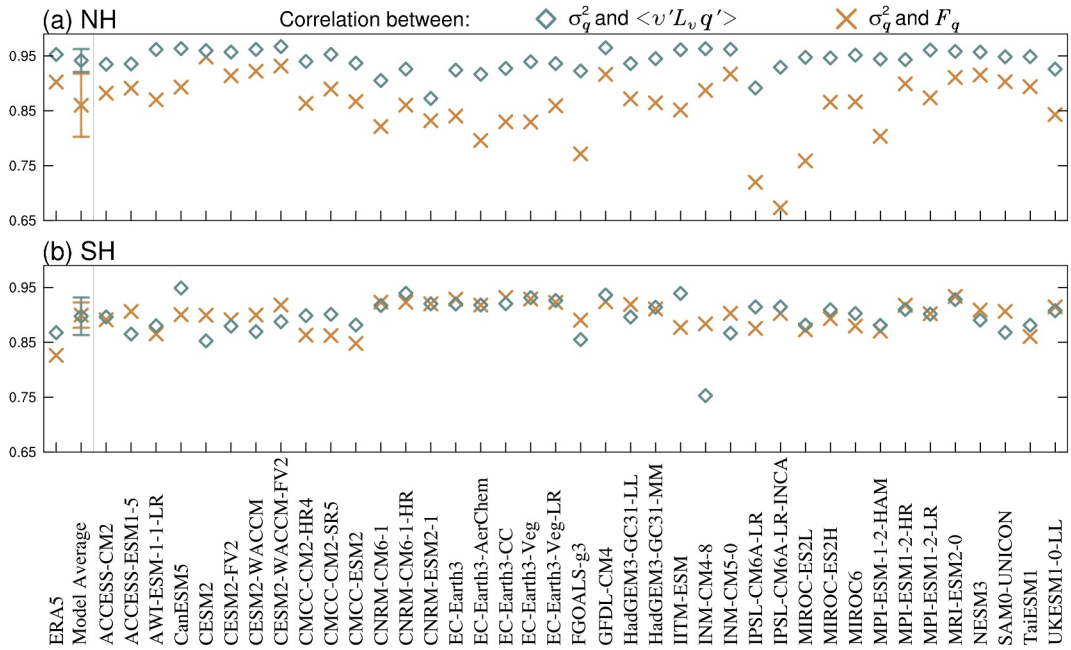

Figure 4. Correlation coefficients between tropical depression (TD)-filtered moisture variance and poleward eddy moisture flux (σ_q^2 and $\langle v' L_v q' \rangle$; diamond markers), and between TD-filtered moisture variance and $F_q \equiv -fS^{-1}\partial_y L_v \overline{P}$ (cross markers), for the (a) Northern Hemisphere and (b) Southern Hemisphere, summarizing the analysis as shown in Figures 3a–3d, but for ERA5 and 39 CMIP6 models. Error bar represents one standard deviation of model results.

included, yielding a multi-model mean of 0.90 ± 0.02. Similar results are also seen in models when considering definitions of F_q based on vertical velocity or Ψ (Figure S7 in Supporting Information S1).

The strong coherence between TD-type variability and instability metric is evident in most models. This leads to the question of whether models with higher F_q values simulate stronger wave variability. To assess this, we perform an intermodel comparison of instability metric and wave activity, presented in Figure 5. Values of models and reanalysis are averaged over specific regions and seasons: Northern Hemisphere (10°N–30°N, June–November) and Southern Hemisphere (10°S–30°S, December–May). Figure 5a shows a significant correlation between TD variance and $\langle v' L_v q' \rangle$ in the Northern Hemisphere ($\gamma = 0.90$). A similar relation is also seen in the Southern Hemisphere ($\gamma = 0.73$, Figure 5b). Eddy moisture flux is well-correlated with F_q in the Northern Hemisphere ($\gamma = 0.55$, Figure 5c). Over the Southern Hemisphere, the association between $\langle v' L_v q' \rangle$ and F_q is not statistically significant (Figure 5d). Interestingly, we find correlations that are higher and statistically significant in this hemisphere if we use definitions of F_q based on vertical velocity and Ψ instead (see Figure S8 in Supporting Information S1). Nonetheless, all examined relations for $\langle v' L_v q' \rangle$ and F_q are statistically significant according to their rank correlations, suggesting that models with higher F_q tend to simulate stronger TD-type wave activity. Similar results to those shown in Figure 5 and Figure S8 in Supporting Information S1 are found when we compare σ_q^2 and F_q, although the correlations are lower (Figure S9 in Supporting Information S1). The uncertainty in the Southern Hemisphere likely stems from the relatively weak TD-type wave variability (Hollis et al., 2024) and potentially unrealistic rainfall simulations in that hemisphere (Brown et al., 2013; Liu & Grise, 2023). It is also possible that Southern Hemisphere TD-type wave variability is more closely connected with extratropical forcing, which is strong year-round.

6. Summary and Conclusions

This study aimed to determine whether TD-type waves grow from instabilities associated with the Hadley Cell, following the theoretical framework proposed by Adames Corraliza and Mayta (2024). To address this hypothesis, we posed two key questions, the answers to which are summarized below.

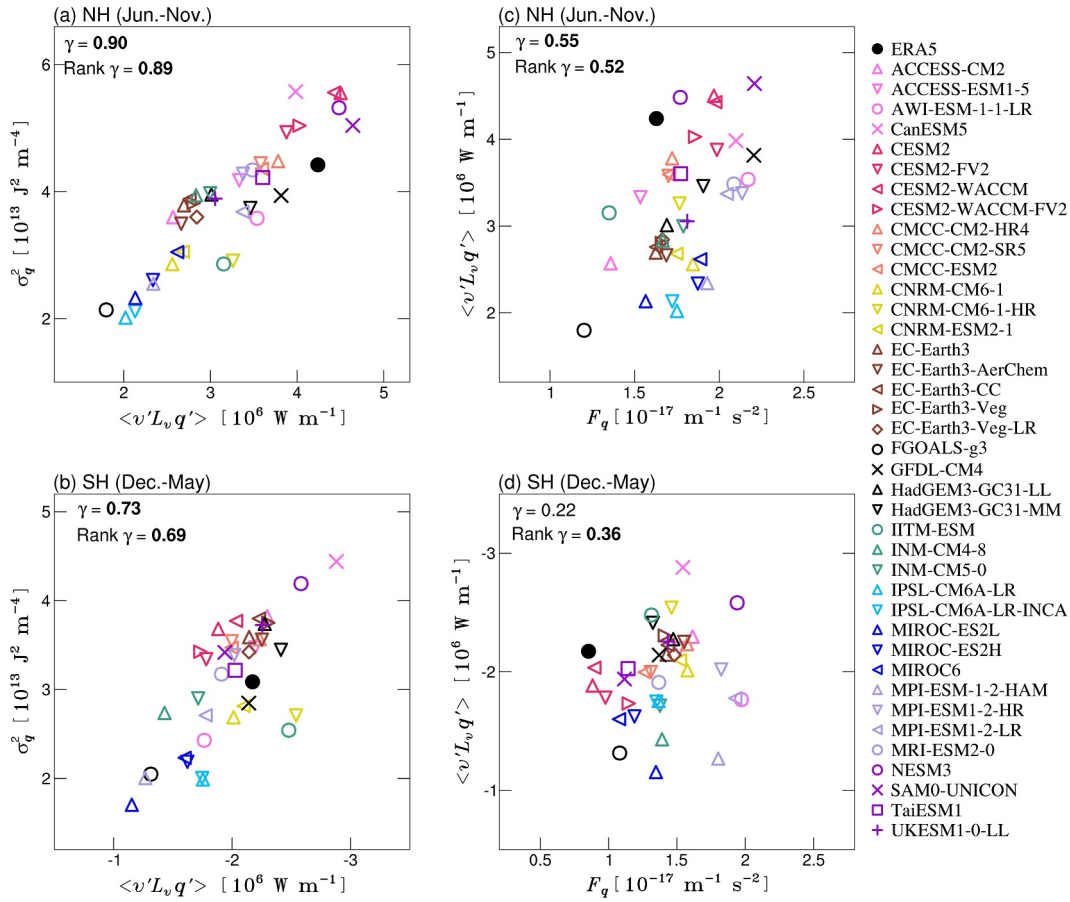

Figure 5. Scatterplots of (a) $\langle v'L_v q' \rangle$ versus σ_q^2 and (c) $F_q \equiv -fS^{-1}\partial_y L_v \overline{P}$ versus $\langle v'L_v q' \rangle$, for ERA5 and 39 CMIP6 models, averaged over the Northern Hemisphere (10°N–30°N) from June to November. As (a, c), but (b, d) averaged over the Southern Hemisphere (10°S–30°S) from December to May. Values in the top-left corner are correlation coefficients (γ) and Spearman's rank correlation coefficient (rank γ), based on results from 39 models. Bold values indicate correlations significant at the 95% confidence level (p-value <0.05). The Southern Hemisphere's axis values are smaller than those of the Northern Hemisphere.

Q1: How is the TD-type wave variability linked to the Hadley Cell?

Consistent with theory (Adames Corraliza & Mayta, 2024), the strength of TD-type wave variability is correlated with a Hadley Cell instability metric defined as F_q (Figures 2 and 3), a diagnostic quantity closely tied to the combined effects of the mean meridional moisture gradient and the sensitivity of rainfall to moisture fluctuations, which in turn links to the background precipitation and the Hadley Cell's streamfunction. The maximum amplification of TD-type waves occurs when the Hadley Cell is at its most weak and narrow, coinciding with peak F_q values (Figure 3 and Figure S6 in Supporting Information S1). The observed stronger TD-type wave intensity in the Northern Hemisphere (Hollis et al., 2024) can be attributed to the larger F_q in this hemisphere. Thus, according to moisture mode/MVI theory, the Northern Hemisphere is more unstable to TD-type variability than the Southern Hemisphere. This consistency is further supported by the seasonality of TD-filtered curvature vorticity (see Section S3 in Supporting Information S1). Beyond the seasonal cycle, we find that F_q also influences the interannual variability of TD-type waves (refer to Section S4 in Supporting Information S1 for further discussion).

Q2: To what extent can global climate models reproduce this association?

All climate models analyzed in this study consistently capture the correlation between TD-type wave variability and F_q in both hemispheres (Figure 4). Furthermore, a multi-model comparison reveals that stronger TD-type activity during the Northern Hemisphere summer is associated with more intense F_q, highlighting the

importance of F_q for realistic simulations (Figure 5). Although weaker, a similar association is also detected in the Southern Hemisphere.

While this study documents an association between TD-type waves and the Hadley Cell, some issues remain open for future investigation. The mean meridional moisture gradient poleward of the ITCZ is weakest during summer (Figure S1 in Supporting Information S1), although the precipitation gradient is strongest. This implies that the large instability seen during summer is a result of a higher sensitivity of rainfall to column moisture (shorter τ_c), as expected from the empirical precipitation-moisture relation (Bretherton et al., 2004). Although this result can be interpreted using existing theory (Ahmed et al., 2020; Emanuel, 2019), it has not been tied to the Hadley Cell or TD-type wave. More work is needed to understand precipitation sensitivity to moisture and its relation to the tropical variability, the mean circulation, and convective parameterizations. On the other hand, model biases–such as uncertainties in warm pool size or the presence of a double ITCZ (Liu & Grise, 2023; Tian & Dong, 2020)–could alter the horizontal gradient of the ITCZ rainfall, thereby affecting Hadley Cell instability metric. It is therefore worth assessing how these biases influence both the instability mechanism and the simulation of tropical disturbances.

The results of this study can help clarify the role of TD-type waves in the tropical circulation. Existing evidence suggests that TD-type waves contribute to ITCZ breakdown (Bembenek et al., 2021; Nieto Ferreira & Schubert, 1997) and are linked to convective aggregation-disaggregation cycles (Tompkins et al., 2024). How the framework proposed here integrates with these existing mechanisms remains to be explored.

These results also provide insights into how TD-like waves may respond to a warming climate. While previous studies have examined these waves in specific locations (Huangfu et al., 2022; Sandeep et al., 2018), a comprehensive global assessment has not been conducted. The proposed theoretical framework can be further tested using idealized experiments to understand how TD-type waves are represented across different climate models. In addition, the interannual correlation between F_q and TD-type wave activity shown in Figure S5 in Supporting Information S1 suggests that the framework may help explain the modulation of TD-type waves by phenomena such as the MJO and El Niño (Huang & Huang, 2011; Rydbeck & Maloney, 2015). All of these represent potentially insightful directions for future research.

Data Availability Statement

ERA5 reanalysis data was accessed and downloaded through Copernicus Climate Change Service Climate Data Store (Hersbach et al., 2023). We downloaded the CMIP6 model simulation outputs from the Lawrence Livermore National Laboratory (https://esgf-node.llnl.gov/search/cmip6, accessed on 31 July 2022) and the Deutsches Klimarechenzentrum (https://esgf-metagrid.cloud.dkrz.de/search/cmip6-dkrz/, accessed on 20 July 2024).

Acknowledgments
QJL and ÁFAC were supported by NSF CAREER Grant 2236433. VCM was supported by NOAA Grants NA22OAR4310611 and NA24OARX431G0049. We thank the two anonymous reviewers for their valuable comments that helped improve the contents of this manuscript.

References

Adames, Á. F. (2021). Interactions between water vapor, potential vorticity, and vertical wind shear in quasi-geostrophic motions: Implications for rotational tropical motion systems. *Journal of the Atmospheric Sciences*, *78*(3), 903–923. https://doi.org/10.1175/jas-d-20-0205.1

Adames, Á. F., & Ming, Y. (2018). Interactions between water vapor and potential vorticity in synoptic-scale monsoonal disturbances: Moisture vortex instability. *Journal of the Atmospheric Sciences*, *75*(6), 2083–2106. https://doi.org/10.1175/jas-d-17-0310.1

Adames Corraliza, Á. F., & Mayta, V. C. (2024). The stirring tropics: Theory of moisture mode–Hadley Cell interactions. *Journal of Climate*, *37*(4), 1383–1401. https://doi.org/10.1175/jcli-d-23-0147.1

Ahmed, F., Adames, Á. F., & Neelin, J. D. (2020). Deep convective adjustment of temperature and moisture. *Journal of the Atmospheric Sciences*, *77*(6), 2163–2186. https://doi.org/10.1175/jas-d-19-0227.1

Ahmed, F., Neelin, J. D., & Adames, Á. F. (2021). Quasi-equilibrium and weak temperature gradient balances in an equatorial beta-plane model. *Journal of the Atmospheric Sciences*, *78*(1), 209–227. https://doi.org/10.1175/jas-d-20-0184.1

Avila, L. A., Pasch, R. J., & Jiing, J.-G. (2000). Atlantic tropical systems of 1996 and 1997: Years of contrasts. *Monthly Weather Review*, *128*(10), 3695–3706. https://doi.org/10.1175/1520-0493(2000)128<3695:atsoay>2.0.co;2

Bembenek, E., Merlis, T. M., & Straub, D. N. (2021). Influence of latitude and moisture effects on the barotropic instability of an idealized ITCZ. *Journal of the Atmospheric Sciences*, *78*(9), 2677–2689. https://doi.org/10.1175/jas-d-20-0346.1

Bretherton, C. S., Peters, M. E., & Back, L. E. (2004). Relationships between water vapor path and precipitation over the tropical oceans. *Journal of Climate*, *17*(7), 1517–1528. https://doi.org/10.1175/1520-0442(2004)017<1517:rbwvpa>2.0.co;2

Brown, J. R., Moise, A. F., & Colman, R. A. (2013). The South Pacific convergence zone in CMIP5 simulations of historical and future climate. *Climate Dynamics*, *41*(7–8), 2179–2197. https://doi.org/10.1007/s00382-012-1591-x

Caballero, R. (2007). Role of eddies in the interannual variability of Hadley Cell strength. *Geophysical Research Letters*, *34*(22), L22705. https://doi.org/10.1029/2007gl030971

Camargo, S. J. (2013). Global and regional aspects of tropical cyclone activity in the CMIP5 models. *Journal of Climate*, *26*(24), 9880–9902. https://doi.org/10.1175/JCLI-D-12-00549.1

Chemke, R., & Polvani, L. M. (2019). Opposite tropical circulation trends in climate models and in reanalyses. *Nature Geoscience*, *12*(7), 528–532. https://doi.org/10.1038/s41561-019-0383-x

Cheng, Y.-M., Dias, J., Kiladis, G., Feng, Z., & Leung, L. R. (2023). Mesoscale convective systems modulated by convectively coupled equatorial waves. *Geophysical Research Letters*, *50*(10), e2023GL103335. https://doi.org/10.1029/2023gl103335

Chikira, M. (2014). Eastward-propagating intraseasonal oscillation represented by Chikira–Sugiyama cumulus parameterization. Part II: Understanding moisture variation under weak temperature gradient balance. *Journal of the Atmospheric Sciences*, *71*(2), 615–639. https://doi.org/10.1175/jas-d-13-038.1

Daloz, A. S., Chauvin, F., Walsh, K., Lavender, S., Abbs, D., & Roux, F. (2012). The ability of general circulation models to simulate tropical cyclones and their precursors over the North Atlantic main development region. *Climate Dynamics*, *39*(7–8), 2666–2684. https://doi.org/10.1007/s00382-012-1290-7

Dias, J., Gehne, M., Kiladis, G. N., & Magnusson, L. (2023). The role of convectively coupled equatorial waves in sub-seasonal predictions. *Geophysical Research Letters*, *50*(21), e2023GL106198. https://doi.org/10.1029/2023gl106198

Dias, J., & Kiladis, G. N. (2014). Influence of the basic state zonal flow on convectively coupled equatorial waves. *Geophysical Research Letters*, *41*(19), 6904–6913. https://doi.org/10.1002/2014gl061476

Dominguez, C., Done, J. M., & Bruyère, C. L. (2020). Easterly wave contributions to seasonal rainfall over the tropical Americas in observations and a regional climate model. *Climate Dynamics*, *54*(1), 191–209. https://doi.org/10.1007/s00382-019-04996-7

Donnelle, D., & Rust, B. (2005). The fast Fourier transform for experimentalists. Part I. Concepts. *Computing in Science & Engineering*, *7*(2), 80–88. https://doi.org/10.1109/mcse.2005.42

Emanuel, K. (2019). Inferences from simple models of slow, convectively coupled processes. *Journal of the Atmospheric Sciences*, *76*(1), 195–208. https://doi.org/10.1175/jas-d-18-0090.1

Eyring, V., Bony, S., Meehl, G. A., Senior, C. A., Stevens, B., Stouffer, R. J., & Taylor, K. E. (2016). Overview of the coupled model intercomparison project phase 6 (CMIP6) experimental design and organization. *Geoscientific Model Development*, *9*(5), 1937–1958. https://doi.org/10.5194/gmd-9-1937-2016

Frank, W. M., & Roundy, P. E. (2006). The role of tropical waves in tropical cyclogenesis. *Monthly Weather Review*, *134*(9), 2397–2417. https://doi.org/10.1175/mwr3204.1

Hersbach, H., Bell, B., Berrisford, P., Biavati, G., Horányi, A., Muñoz Sabater, J., et al. (2023). ERA5 hourly data on pressure levels from 1940 to present [Dataset]. *Copernicus Climate Change Service (C3S) Climate Data Store (CDS)*. https://doi.org/10.24381/cds.bd0915c6

Hersbach, H., Bell, B., Berrisford, P., Horányi, A., Sabater, J. M., Nicolas, J., et al. (2019). Global reanalysis: Goodbye ERA-interim, hello ERA5. *ECMWF Newsletter*, *159*, 17–24. Retrieved from https://cir.nii.ac.jp/crid/1370302864780227330

Hollis, M. A., McCrary, R. R., Stachnik, J. P., Lewis-Merritt, C., & Martin, E. R. (2024). A global climatology of tropical easterly waves. *Climate Dynamics*, *62*(3), 2317–2332. https://doi.org/10.1007/s00382-023-07025-w

Huang, P., Chou, C., & Huang, R. (2013). The activity of convectively coupled equatorial waves in CMIP3 global climate models. *Theoretical and Applied Climatology*, *112*(3–4), 697–711. https://doi.org/10.1007/s00704-012-0761-4

Huang, P., & Huang, R. (2011). Climatology and interannual variability of convectively coupled equatorial waves activity. *Journal of Climate*, *24*(16), 4451–4465. https://doi.org/10.1175/2011jcli4021.1

Huangfu, J., Cao, X., Wu, R., Chen, G., & Chen, W. (2022). Influences of central Pacific warming on synoptic-scale wave intensity over the northwest Pacific. *Climate Dynamics*, *58*(1), 555–567. https://doi.org/10.1007/s00382-021-05922-6

Jones, P. W. (1999). First-and second-order conservative remapping schemes for grids in spherical coordinates. *Monthly Weather Review*, *127*(9), 2204–2210. https://doi.org/10.1175/1520-0493(1999)127<2204:fasocr>2.0.co;2

Kang, S. M., Deser, C., & Polvani, L. M. (2013). Uncertainty in climate change projections of the Hadley circulation: The role of internal variability. *Journal of Climate*, *26*(19), 7541–7554. https://doi.org/10.1175/jcli-d-12-00788.1

Kiladis, G. N., Thorncroft, C. D., & Hall, N. M. (2006). Three-dimensional structure and dynamics of African easterly waves. Part I: Observations. *Journal of the Atmospheric Sciences*, *63*(9), 2212–2230. https://doi.org/10.1175/jas3741.1

Kiladis, G. N., Wheeler, M. C., Haertel, P. T., Straub, K. H., & Roundy, P. E. (2009). Convectively coupled equatorial waves. *Reviews of Geophysics*, *47*(2), RG2003. https://doi.org/10.1029/2008rg000266

Landsea, C. W. (1993). A climatology of intense (or major) Atlantic hurricanes. *Monthly Weather Review*, *121*(6), 1703–1713. https://doi.org/10.1175/1520-0493(1993)121<1703:acoima>2.0.co;2

Lau, K.-H., & Lau, N.-C. (1990). Observed structure and propagation characteristics of tropical summertime synoptic scale disturbances. *Monthly Weather Review*, *118*(9), 1888–1913. https://doi.org/10.1175/1520-0493(1990)118<1888:osapco>2.0.co;2

Liu, X., & Grise, K. M. (2023). Implications of warm pool bias in CMIP6 models on the Northern Hemisphere wintertime subtropical jet and precipitation. *Geophysical Research Letters*, *50*(15), e2023GL104896. https://doi.org/10.1029/2023gl104896

Lubis, S. W., & Jacobi, C. (2015). The modulating influence of convectively coupled equatorial waves (CCEWs) on the variability of tropical precipitation. *International Journal of Climatology*, *35*(7), 1465–1483. https://doi.org/10.1002/joc.4069

Luo, H., Adames Corraliza, Á. F., & Rood, R. B. (2023). Barotropic and moisture–vortex growth of monsoon low pressure systems. *Journal of the Atmospheric Sciences*, *80*(12), 2823–2836. https://doi.org/10.1175/jas-d-22-0252.1

Martin, E. R., & Thorncroft, C. (2015). Representation of African easterly waves in CMIP5 models. *Journal of Climate*, *28*(19), 7702–7715. https://doi.org/10.1175/JCLI-D-15-0145.1

Matsuno, T. (1966). Quasi-geostrophic motions in the equatorial area. *Journal of the Meteorological Society of Japan. Ser. II*, *44*(1), 25–43. https://doi.org/10.2151/jmsj1965.44.1_25

Mayta, V. C., & Adames, Á. F. (2023). Moist thermodynamics of convectively coupled waves over the Western Hemisphere. *Journal of Climate*, *36*(9), 2765–2780. https://doi.org/10.1175/jcli-d-22-0435.1

Mayta, V. C., Adames, Á. F., & Ahmed, F. (2022). Westward-propagating moisture mode over the tropical Western Hemisphere. *Geophysical Research Letters*, *49*(6), e2022GL097799. https://doi.org/10.1029/2022gl097799

Mayta, V. C., & Adames Corraliza, Á. F. (2024). The stirring tropics: The ubiquity of moisture modes and moisture–vortex instability. *Journal of Climate*, *37*(6), 1981–1998. https://doi.org/10.1175/jcli-d-23-0145.1

Mayta, V. C., Adames Corraliza, Á. F., Lin, Q.-J., & Vargas Martes, R. M. (2025). Caribbean easterly waves: Structure, thermodynamics, and instability mechanisms. *Journal of the Atmospheric Sciences*, *82*(7), 1451–1465. https://doi.org/10.1175/jas-d-24-0232.1

Mitas, C. M., & Clement, A. (2005). Has the Hadley Cell been strengthening in recent decades? *Geophysical Research Letters*, *32*(3), L03809. https://doi.org/10.1029/2004gl021765

Nieto Ferreira, R., & Schubert, W. H. (1997). Barotropic aspects of ITCZ breakdown. *Journal of the Atmospheric Sciences*, *54*(2), 261–285. https://doi.org/10.1175/1520-0469(1997)054<0261:baoib>2.0.co;2

Nitta, T., Nakagomi, Y., Suzuki, Y., Hasegawa, N., & Kadokura, A. (1985). Global analysis of the lower tropospheric disturbances in the tropics during the northern summer of the FGGE year. Part I: Global features of the disturbances. *Journal of the Meteorological Society of Japan. Ser. II*, *63*(1), 1–19. https://doi.org/10.2151/jmsj1965.63.1_1

Oort, A. H., & Yienger, J. J. (1996). Observed interannual variability in the Hadley circulation and its connection to ENSO. *Journal of Climate*, *9*(11), 2751–2767. https://doi.org/10.1175/1520-0442(1996)009<2751:oivith>2.0.co;2

Peters, M. E., & Bretherton, C. S. (2005). A simplified model of the walker circulation with an interactive ocean mixed layer and cloud-radiative feedbacks. *Journal of Climate*, *18*(20), 4216–4234. https://doi.org/10.1175/jcli3534.1

Pikovnik, M., Zaplotnik, Ž., Boljka, L., & Žagar, N. (2022). Metrics of the Hadley circulation strength and associated circulation trends. *Weather and Climate Dynamics*, *3*(2), 625–644. https://doi.org/10.5194/wcd-3-625-2022

Raymond, D. J., & Fuchs, Ž. (2009). Moisture modes and the Madden–Julian Oscillation. *Journal of Climate*, *22*(11), 3031–3046. https://doi.org/10.1175/2008jcli2739.1

Reed, R. J., & Recker, E. E. (1971). Structure and properties of synoptic-scale wave disturbances in the equatorial Western Pacific. *Journal of the Atmospheric Sciences*, *28*(7), 1117–1133. https://doi.org/10.1175/1520-0469(1971)028<1117:saposs>2.0.co;2

Riehl, H. (1945). *Waves in the easterlies and the polar front in the tropics*. University of Chicago Press.

Russell, J. O., Aiyyer, A., White, J. D., & Hannah, W. (2017). Revisiting the connection between African easterly waves and Atlantic tropical cyclogenesis. *Geophysical Research Letters*, *44*(1), 587–595. https://doi.org/10.1002/2016gl071236

Ruti, P. M., & Dell' Aquila, A. (2010). The twentieth century African easterly waves in reanalysis systems and IPCC simulations, from intra-seasonal to inter-annual variability. *Climate Dynamics*, *35*(6), 1099–1117. https://doi.org/10.1007/s00382-010-0894-z

Rydbeck, A. V., & Maloney, E. D. (2014). Energetics of east Pacific easterly waves during intraseasonal events. *Journal of Climate*, *27*(20), 7603–7621. https://doi.org/10.1175/jcli-d-14-00211.1

Rydbeck, A. V., & Maloney, E. D. (2015). On the convective coupling and moisture organization of east Pacific easterly waves. *Journal of the Atmospheric Sciences*, *72*(10), 3850–3870. https://doi.org/10.1175/jas-d-15-0056.1

Sandeep, S., Ajayamohan, R., Boos, W. R., Sabin, T., & Praveen, V. (2018). Decline and poleward shift in Indian summer monsoon synoptic activity in a warming climate. *Proceedings of the National Academy of Sciences of the United States of America*, *115*(11), 2681–2686. https://doi.org/10.1073/pnas.1709031115

Schneider, T., O'Gorman, P. A., & Levine, X. J. (2010). Water vapor and the dynamics of climate changes. *Reviews of Geophysics*, *48*(3), RG3001. https://doi.org/10.1029/2009rg000302

Serra, Y. L., Kiladis, G. N., & Hodges, K. I. (2010). Tracking and mean structure of easterly waves over the intra-Americas Sea. *Journal of Climate*, *23*(18), 4823–4840. https://doi.org/10.1175/2010jcli3223.1

Shapiro, L. J. (1986). The three-dimensional structure of synoptic-scale disturbances over the tropical Atlantic. *Monthly Weather Review*, *114*(10), 1876–1891. https://doi.org/10.1175/1520-0493(1986)114<1876:ttdsos>2.0.co;2

Skinner, C. B., & Diffenbaugh, N. S. (2013). The contribution of African easterly waves to monsoon precipitation in the CMIP3 ensemble. *Journal of Geophysical Research: Atmospheres*, *118*(9), 3590–3609. https://doi.org/10.1002/jgrd.50363

Skinner, C. B., & Diffenbaugh, N. S. (2014). Projected changes in African easterly wave intensity and track in response to greenhouse forcing. *Proceedings of the National Academy of Sciences of the United States of America*, *111*(19), 6882–6887. https://doi.org/10.1073/pnas.1319597111

Sobel, A., & Maloney, E. (2012). An idealized semi-empirical framework for modeling the Madden–Julian Oscillation. *Journal of the Atmospheric Sciences*, *69*(5), 1691–1705. https://doi.org/10.1175/jas-d-11-0118.1

Sobel, A. H., & Bretherton, C. S. (1999). Development of synoptic-scale disturbances over the summertime tropical northwest Pacific. *Journal of the Atmospheric Sciences*, *56*(17), 3106–3127. https://doi.org/10.1175/1520-0469(1999)056<3106:dossdo>2.0.co;2

Sobel, A. H., Nilsson, J., & Polvani, L. M. (2001). The weak temperature gradient approximation and balanced tropical moisture waves. *Journal of the Atmospheric Sciences*, *58*(23), 3650–3665. https://doi.org/10.1175/1520-0469(2001)058<3650:twtgaa>2.0.co;2

Takayabu, Y. N. (1994). Large-scale cloud disturbances associated with equatorial waves part I: Spectral features of the cloud disturbances. *Journal of the Meteorological Society of Japan. Ser. II*, *72*(3), 433–449. https://doi.org/10.2151/jmsj1965.72.3_433

Takayabu, Y. N., & Nitta, T. (1993). 3-5 day-period disturbances coupled with convection over the tropical Pacific Ocean. *Journal of the Meteorological Society of Japan. Ser. II*, *71*(2), 221–246. https://doi.org/10.2151/jmsj1965.71.2_221

Tian, B., & Dong, X. (2020). The double-ITCZ bias in CMIP3, CMIP5, and CMIP6 models based on annual mean precipitation. *Geophysical Research Letters*, *47*(8), e2020GL087232. https://doi.org/10.1029/2020gl087232

Tompkins, A., Casallas, A., & de Vera, M. (2024). Drivers of mesoscale convective aggregation and spatial humidity variability in the tropical western Pacific.

Vargas Martes, R. M., Adames Corraliza, Á. F., & Mayta, V. C. (2023). The role of water vapor and temperature in the thermodynamics of tropical northeast Pacific and African easterly waves. *Journal of the Atmospheric Sciences*, *80*(9), 2305–2322. https://doi.org/10.1175/jas-d-22-0177.1

Vargas Martes, R. M., Adames Corraliza, Á. F., Mayta, V. C., & Lin, Q.-J. (2025). East Pacific easterly wave representation in CMIP6 models. *Geophysical Research Letters*, *52*(8), e2024GL113233. https://doi.org/10.1029/2024GL113233

Wheeler, M., & Kiladis, G. N. (1999). Convectively coupled equatorial waves: Analysis of clouds and temperature in the wavenumber–frequency domain. *Journal of the Atmospheric Sciences*, *56*(3), 374–399. https://doi.org/10.1175/1520-0469(1999)056<0374:ccewao>2.0.co;2

Wolding, B. O., & Maloney, E. D. (2015). Objective diagnostics and the Madden–Julian oscillation. Part II: Application to moist static energy and moisture budgets. *Journal of Climate*, *28*(19), 7786–7808. https://doi.org/10.1175/jcli-d-14-00689.1

Wolding, B. O., Maloney, E. D., & Branson, M. (2016). Vertically resolved weak temperature gradient analysis of the Madden-Julian Oscillation in SP-CESM. *Journal of Advances in Modeling Earth Systems*, *8*(4), 1586–1619. https://doi.org/10.1002/2016MS000724

Yoshida, R., & Ishikawa, H. (2013). Environmental factors contributing to tropical cyclone genesis over the western North Pacific. *Monthly Weather Review*, *141*(2), 451–467. https://doi.org/10.1175/mwr-d-11-00309.1

Yu, J.-Y., & Neelin, J. D. (1994). Modes of tropical variability under convective adjustment and the Madden–Julian Oscillation. Part II: Numerical results. *Journal of the Atmospheric Sciences*, *51*(13), 1895–1914. https://doi.org/10.1175/1520-0469(1994)051<1895:motvuc>2.0.co;2

References From the Supporting Information

Adames, Á. F. (2017). Precipitation budget of the Madden–Julian Oscillation. *Journal of the Atmospheric Sciences*, *74*(6), 1799–1817. https://doi.org/10.1175/jas-d-16-0242.1

Du, X., Chu, J.-E., Jin, F.-F., & Cheung, H. M. (2025). Global coupled dynamics of tropical easterly waves and tropical cyclone genesis. *npj Climate and Atmospheric Science*, *8*(1), 125. https://doi.org/10.1038/s41612-025-01014-y

Inoue, K., & Back, L. E. (2015). Gross moist stability assessment during TOGA COARE: Various interpretations of gross moist stability. *Journal of the Atmospheric Sciences*, *72*(11), 4148–4166. https://doi.org/10.1175/jas-d-15-0092.1

Inoue, K., Biasutti, M., & Fridlind, A. M. (2021). Evidence that horizontal moisture advection regulates the ubiquitous amplification of rainfall variability over tropical oceans. *Journal of the Atmospheric Sciences*, *78*(2), 529–547. https://doi.org/10.1175/jas-d-20-0201.1

Maithel, V., & Back, L. (2022). Moisture recharge–discharge cycles: A gross moist stability–based phase angle perspective. *Journal of the Atmospheric Sciences*, *79*(9), 2401–2417. https://doi.org/10.1175/jas-d-21-0297.1